Data-Centric Engineering (2026), 7: e3
doi:10.1017/dce.2026.10037

CAMBRIDGE UNIVERSITY PRESS

RESEARCH ARTICLE

A Bayesian optimization approach for reliability-based design of prestressed concrete structures

James Whiteley and Jurgen Becque

Engineering Department, University of Cambridge, UK
Corresponding author: James Whiteley; Email: jw2293@cam.ac.uk

Received: 28 July 2025; **Revised:** 13 November 2025; **Accepted:** 09 December 2025

Keywords: Bayesian optimization; Gaussian process; prestressed concrete; reliability-based design optimization; structural optimization

Abstract

This paper presents a reliability-constrained Bayesian optimization framework for structural design under uncertainty, addressing challenges in stochastic optimization where the objectives and constraints are defined implicitly by potentially expensive numerical models. Our approach explicitly accounts for parameter uncertainty using results from Bayesian quadrature for uncertainty propagation in Gaussian process surrogate models. The method accommodates arbitrary probability distributions and employs gradient-based optimization for acquisition function maximization, strategically selecting sample points to minimize numerical model evaluations. We demonstrate our algorithm's superior performance over random search and conventional Bayesian optimization through both an analytical test function and a prestressed tie-beam design case study, showing its practical applicability to structural optimization problems.

Impact Statement

This research addresses a current challenge in structural engineering of increasing importance: designing efficient and reliable structures in the face of uncertainty—a key consideration in reducing the carbon footprint of construction. Our framework offers a simple but effective solution to the computational challenges of reliability-based design optimization that works well in low dimensions. Since the method is agnostic to the type of numerical structural model used, the approach is applicable to many problems beyond the presented example on prestressed concrete design. Ultimately, this work contributes to the development of a more sustainable built environment by enabling more efficient use of materials while explicitly maintaining adequate safety standards.

1. Introduction

Uncertainty in the context of structural engineering exists in material properties, environmental conditions, and structural geometry, as well as within structural analysis models and as a result of human error. Ambiguity in these quantities arises from either a lack of data or due to inherent randomness (Faber and Sørensen, 2002). Modern building codes, such as the Eurocodes (CEN, 2002), deal with uncertainties in

This research article was awarded Open Data and Open Materials badges for transparent practices. See the Data Availability Statement for details.

© The Author(s), 2026. Published by Cambridge University Press. This is an Open Access article, distributed under the terms of the Creative Commons Attribution licence (http://creativecommons.org/licenses/by/4.0), which permits unrestricted re-use, distribution and reproduction, provided the original article is properly cited.

https://doi.org/10.1017/dce.2026.10037 Published online by Cambridge University Press

design by adopting a load and resistance factor approach, first introduced by Ellingwood in the early 1980s (Ellingwood et al., 1982), which applies factors of safety (termed partial safety factors) to both loads and resistances. While modern codes have been highly successful in delivering high standards of safety and performance in design, they possess a number of limitations. Partial safety factors are deterministic and only implicitly account for the probabilistic nature of loads and material strengths. In applying partial safety factors uniformly across a wide range of structure types and construction practices, it is likely that there exists over-conservatism in design in some scenarios and under-conservatism in others. Structural engineering as a profession has accumulated a wealth of implicit knowledge based on historic trial and error. This has helped form the basis of the calibration of code partial safety factors (Faber and Sørensen, 2002), which are to some extent subjective. In light of climate goals, it may be warranted to reconsider the trade-offs between safety and efficiency in design.

One approach to design structures whilst explicitly accounting for uncertainty is reliability-based design optimization (Hu et al., 2024). In contrast to deterministic optimization, which assumes fixed values for parameters, reliability-based optimization accounts for variability in inputs. Specifically, probabilistic constraints (also known as chance constraints) are used to ensure the design achieves a desired level of reliability. Reliability-based optimization problems are difficult to solve: they are generally non-convex, even if the underlying functions in the constraint and objective are convex, and hence it cannot be guaranteed that a local minimum is the global optimum (Campi and Garatti, 2011). In addition, checking the feasibility of objectives and constraints is computationally expensive because it requires multivariate integration, which is an NP-hard problem (Khachiyan, 1989). Classical methods used to solve reliability-based optimization within the discipline of engineering have been developed extensively since the 1960s (Hilton and Feigen, 1960). These methods typically rely on deterministic approximations to evaluate system reliability and struggle to model complex, highly nonlinear systems. Whilst simulation-based approaches (such as Monte Carlo simulation) alleviate this issue, they can be prohibitively expensive where computationally demanding numerical models define the optimization objective or constraints. To address these challenges, machine learning surrogate modeling—where a sample-efficient model trained on data replaces the expensive simulation—has emerged as a powerful tool for simulation-based reliability assessment (Moustapha and Sudret, 2019). The use of these surrogate models, however, can still require numerous simulations to generate training data. Consequently, a number of studies have explored using Bayesian optimization, which strategically selects training points to minimize the number of model evaluations needed, to optimize engineering systems under uncertainty with minimal computational cost.

In this paper, we focus on reliability-constrained Bayesian optimization, an extension of standard Bayesian optimization that incorporates objectives and constraints expressed probabilistically. In this framework, engineers can optimize designs while accounting for statistical uncertainty in the input parameters. We base our work upon recent advances in reliability-constrained Bayesian optimization. A number of studies have investigated this topic, either from an engineering design perspective, where it is generally referred to as robust design (Apley et al., 2006; Arendt et al., 2013; Do et al., 2021; Zhang et al., 2013) or from a computer science perspective, where phrases such as optimization "with expensive integrands" or "of integrated response functions" are common (Groot et al., 2010; Swersky et al., 2013; Tesch et al., 2011; Toscano-Palmerin and Frazier, 2022; Williams et al., 2000). In the former case, optimization of a statistical measure (e.g., mean, or mean and variance) of an engineering system, given varying environmental conditions, leads to a reliability-based or robust design optimization problem (Arendt et al., 2013; Daulton et al., 2022; Tesch et al., 2011). In the latter case, optimizing machine learning model hyperparameters across multiple tasks or cross-validation batches is mathematically similar to optimizing the expected value of a random function [in the discrete case] (Swersky et al., 2013; Toscano-Palmerin and Frazier, 2022). These approaches generally utilize modifications of well-known deterministic Bayesian optimization strategies (see Section 3).

Whilst the studies previously mentioned have effectively addressed unconstrained optimization problems under uncertainty, structural design presents unique challenges, where constraints often take precedence over objectives (Mathern et al., 2021). Despite the importance of this field, there have been

https://doi.org/10.1017/dce.2026.10037 Published online by Cambridge University Press

relatively few contributions specifically targeting structural design and its distinctive equations and problem formulations. To our knowledge, no previous research has investigated prestressed concrete design—a key focus of our paper. While Bayesian optimization has been applied to deterministic structural design (Mathern et al., 2021) and in a limited number of reliability-based studies (Do et al., 2021), our work makes several new contributions. First, we expand the application to structural engineering examples, which remain underrepresented in the literature. Second, we implement fast, parallel batch optimization with gradient-based methods, which represents an advancement over earlier robust design approaches (Apley et al., 2006; Arendt et al., 2013; Do et al., 2021; Zhang et al., 2013). Third, we demonstrate how Gaussian process surrogates can successfully model prestressed concrete design in the context of Bayesian optimization.

It is worth distinguishing the proposed framework from existing adaptive reliability analysis approaches (Bichon et al., 2008; Moustapha and Sudret, 2019). These methods use acquisition functions to refine a surrogate near a limit-state boundary for improved failure probability estimation, often within a double-loop optimization process. In contrast, the presented framework integrates reliability assessment within a Bayesian optimization approach: model evaluations are selected to improve the reliability-constrained objective itself, unifying reliability estimation and optimization within a single loop. While a direct quantitative comparison with FORM or SORM-based algorithms (Hu et al., 2024)—classical methods of reliability-based optimization performed by approximating the limit-state surface using first or second-order expansions at the design point—is beyond the scope of this study, the presented results illustrate instead how a Bayesian approach can be applied to practical problems in structural design.

The paper is organized as follows: Section 2 outlines the proposed surrogate modeling and optimization framework; Section 3 describes our implementation; Section 4 shows the results of the method applied to both analytic test functions from the literature and an engineering example; Section 5 discusses the implications of our findings and potential limitations of the approach; and Section 6 concludes the paper with a summary of contributions and suggestions for future work.

2. Reliability-based design optimization

This study is focused on the reliability-based optimization problem described by Equation 2.1. In general, reliability-based optimization aims to maximize some statistical measure whilst ensuring satisfaction of probabilistic constraints. In our case, we maximize the expected value of the function $f(\mathbf{x},\boldsymbol{\xi})$, whilst ensuring that reliability constraints $\mathrm{P}[g_i(\mathbf{x},\boldsymbol{\xi}) \leq 0]$ are satisfied with a specified probability $1-\beta_i$:

$$\max_{\mathbf{x}\in\mathcal{X}} \quad \mathbb{E}[f(\mathbf{x},\boldsymbol{\xi})]$$

$$\mathrm{P}[g_i(\mathbf{x},\boldsymbol{\xi}) \leq 0] \geq 1-\beta_i, \quad i=1,\ldots,m \tag{2.1}$$

In the above Equation (2.1), $\mathbf{x}\in\mathcal{X}\subset\mathbb{R}^d$ are deterministic design variables, and $\boldsymbol{\xi}\in\Xi$ are uncertain parameters drawn from a probability distribution over the domain Ξ. $\mathbb{E}$ and P denote an expected value and a probability, respectively. The optimization objective and constraint functions depend on the uncertain parameters but, in contrast to the design variables, they are not controlled by the optimization procedure. What we refer to as uncertain parameters are also commonly referred to as random environmental variables (Toscano-Palmerin and Frazier, 2022), emphasizing their role as uncontrollable random variables of known distribution. In the context of structural design, the imposed (or variable) load from the occupants of a building is a good example of a random environmental variable: the number of people using a particular building cannot generally be explicitly controlled but a probability distribution representing that load can be estimated with reasonable precision.

It should be noted that alternative formulations of design optimization under uncertainty are possible where the design variables themselves are subject to noise (Zhang et al., 2013; Sui et al., 2015; Daulton et al., 2022), that is, $f(\mathbf{x}+\boldsymbol{\xi})$; however, such formulations are not the focus of this paper. In Equation 2.1, the probabilistic (or chance) constraints are assumed to be statistically independent. The case of correlated

https://doi.org/10.1017/dce.2026.10037 Published online by Cambridge University Press

constraints, which must to satisfied jointly, represents a more complex problem (Do et al., 2021) and is beyond the scope of this paper.

3. Bayesian optimization

Bayesian optimization (BayesOpt) is an approach to global optimization which involves two steps performed sequentially: (1) a surrogate model, based on observed data $\mathcal{D}=\{((\mathbf{x}_i,\boldsymbol{\xi}_i),f(\mathbf{x}_i,\boldsymbol{\xi}_i))\}_{i=1}^{n}$, is created, providing a predictive distribution over unseen points; (2) heuristics (called acquisition functions) are then used to decide where to next sample additional data based on the predictive distribution of the current surrogate model. The acquisition function itself may be multimodal and hence hard to optimize, and so BayesOpt makes sense primarily in the case where the original functions being modeled are expensive or time-consuming. A simple example of BayesOpt is shown in Figure 1; an unknown objective function is sampled at points, which are then used to train a Gaussian process surrogate. The distribution in terms of mean and standard deviation of the surrogate is then used to construct an acquisition function. A tutorial on BayesOpt is provided by Frazier (2018).

3.1. Gaussian process

The canonical surrogate model used in BayesOpt is a Gaussian process, which is briefly described here. A Gaussian process is a collection of random variables, any finite subset of which has a joint Gaussian distribution (Rasmussen and Williams, 2006). A Gaussian process is fully specified by a mean function and covariance function, that is, $\hat{f}(\mathbf{x})\sim\mathcal{GP}(m(\mathbf{x}),k(\mathbf{x},\mathbf{x}'))$. Note that for visual clarity, dependence on ξ has been dropped from the notation in this section; $\mathbf{x}$ can be taken to mean $(\mathbf{x},\xi)$. In the absence of specific knowledge about the underlying trend, the mean function is set to zero, that is, $m(\mathbf{x})=0$, which represents an uninformative prior on the function values. The covariance function $k(\mathbf{x},\mathbf{x}')$ encodes the belief that points $\mathbf{x}_i,\mathbf{x}_j$ that are close in the input space will have similar function values in the output space. The squared exponential covariance function is the most common and is used in this work:

$$k(\mathbf{x},\mathbf{x}')=\sigma_f^2\exp\left(-\frac{|\mathbf{x}-\mathbf{x}'|^2}{2\ell^2}\right) \tag{3.1}$$

which has hyperparameters $\boldsymbol{\theta}=\left(\sigma_f^2,\ell\right)$, obtained by maximizing the log marginal likelihood $\log p(\mathbf{y}|\mathbf{X},\boldsymbol{\theta})$. The log marginal likelihood has a well-known closed-form expression (Rasmussen and Williams, 2006). Given a set of observations $\mathbf{y}=[y_1,\ldots,y_n]^\top\in\mathbb{R}^n$ associated with training inputs $\mathbf{X}=[\mathbf{x}_1,\ldots,\mathbf{x}_n]^\top\in\mathbb{R}^{n\times d}$ and a set of query points $\mathbf{X}^*=\left[\mathbf{x}_1^*,\ldots,\mathbf{x}_k^*\right]^\top\in\mathbb{R}^{k\times d}$, Gaussian process regression provides a posterior predictive distribution $\mathbf{y}^*$ over the query points given by

$$\mathbf{y}^*|\mathbf{X},\mathbf{y},\mathbf{X}^*\sim\mathcal{N}(\boldsymbol{\mu}(\mathbf{X}^*),\boldsymbol{\Sigma}(\mathbf{X}^*)) \tag{3.2}$$

$$\boldsymbol{\mu}(\mathbf{X}^*)=K(\mathbf{X}^*,\mathbf{X})K(\mathbf{X},\mathbf{X})^{-1}\mathbf{y} \tag{3.3}$$

$$\boldsymbol{\Sigma}(\mathbf{X}^*)=K(\mathbf{X}^*,\mathbf{X}^*)-K(\mathbf{X}^*,\mathbf{X})K(\mathbf{X},\mathbf{X})^{-1}K(\mathbf{X},\mathbf{X}^*) \tag{3.4}$$

where $K(\mathbf{X},\mathbf{X})\in\mathbb{R}^{n\times n}$ is the covariance matrix between the previously seen points, with entries $K_{ij}=k\left(\mathbf{x}_i,\mathbf{x}_j\right)$. Similarly, $K(\mathbf{X}^*,\mathbf{X}^*)\in\mathbb{R}^{k\times k}$ is the covariance matrix at the query points, and $K(\mathbf{X}^*,\mathbf{X})\in\mathbb{R}^{k\times n}$ is the cross-covariance matrix between the query points and the previously seen points, with entries $K_{ij}=k\left(\mathbf{x}_i^*,\mathbf{x}_j\right)$. In essence, a Gaussian process (hereafter denoted by a hat symbol such as $\hat{f}$) provides a prediction over unseen points $\mathbf{x}^*$, represented as a Gaussian distribution with a mean and variance $\mathbf{y}^*\sim\mathcal{N}(\mu(\mathbf{x}^*),\sigma^2(\mathbf{x}^*))$.

https://doi.org/10.1017/dce.2026.10037 Published online by Cambridge University Press

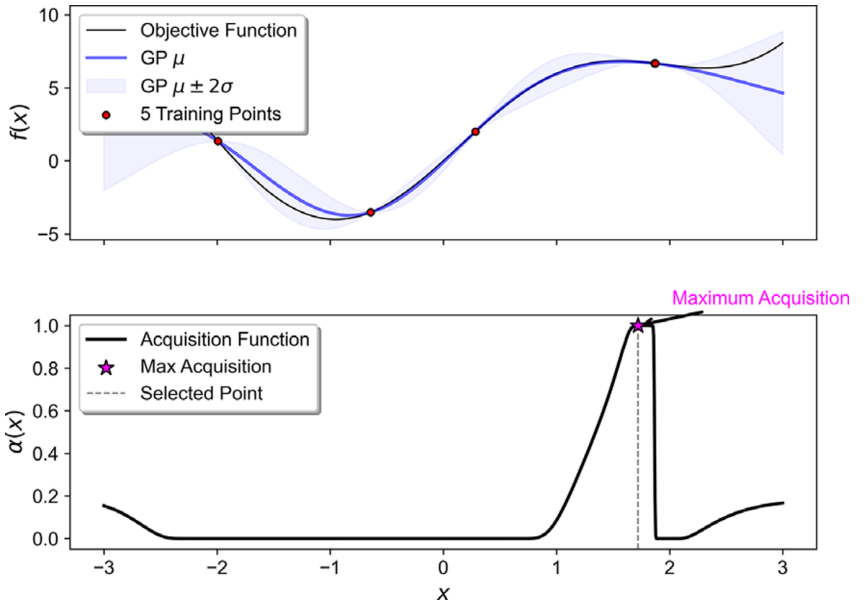


Figure 1. *A simple illustration of Bayesian optimization. A Gaussian process model, trained on four noiseless observations, is visualized, along with the corresponding acquisition function used to select the next evaluation point.*

3.2. Bayes–Hermite quadrature

In the chance-constrained problem defined by Equation 2.1, it is not $f(\mathbf{x},\boldsymbol{\xi})$ itself that one seeks to maximize but rather its expectation over the uncertain parameters $\mathbb{E}[f(\mathbf{x},\boldsymbol{\xi})] = \int f(\mathbf{x},\boldsymbol{\xi})\mathrm{p}(\boldsymbol{\xi})d\boldsymbol{\xi}$. Results from Bayes–Hermite quadrature (O'Hagan, 1991) (or Bayesian Monte Carlo [Rasmussen and Ghahramani, 2003]) provide a means to compute this expectation when a Gaussian process prior $\hat{f}(\mathbf{x},\boldsymbol{\xi}) \sim \mathcal{GP}(m(\mathbf{x},\boldsymbol{\xi}), k((\mathbf{x},\boldsymbol{\xi}),(\mathbf{x}',\boldsymbol{\xi}')))$ is placed over the integrand f. Specifically, for the objective $\overline{f}(\mathbf{x}) = \int \hat{f}(\mathbf{x},\boldsymbol{\xi})p(\boldsymbol{\xi})d\boldsymbol{\xi}$, the posterior distribution $p(\overline{f}|\mathcal{D})$ is Gaussian with mean and covariance:

$$\mathbb{E}_{f|\mathcal{D}}[\overline{f}(\mathbf{x})] = \int \mu(\mathbf{x},\boldsymbol{\xi})p(\boldsymbol{\xi})d\boldsymbol{\xi} := \hat{\mu}(\mathbf{x}) \tag{3.5}$$

$$\mathrm{Cov}_{f|\mathcal{D}}[\overline{f}(\mathbf{x}),\overline{f}(\mathbf{x}')] = \iint \Sigma(\mathbf{x},\boldsymbol{\xi},\mathbf{x}',\boldsymbol{\xi}')p(\boldsymbol{\xi})p(\boldsymbol{\xi}')d\boldsymbol{\xi}d\boldsymbol{\xi}' := \hat{\Sigma}(\mathbf{x},\mathbf{x}') \tag{3.6}$$

where $\mu(\mathbf{x},\boldsymbol{\xi})$ is the posterior mean and $\Sigma(\mathbf{x},\boldsymbol{\xi},\mathbf{x}',\boldsymbol{\xi}')$ the posterior covariance of the Gaussian process $\hat{f}$. Hence, integrating out the uncertain parameters yields a marginal Gaussian process over $\mathbf{x}$ with mean $\hat{\mu}(\mathbf{x})$ and covariance $\hat{\Sigma}(\mathbf{x},\mathbf{x}')$. If the covariance function $k(\mathbf{x},\mathbf{x}')$ and density $p(\boldsymbol{\xi})$ are both Gaussian, analytic results exist for $\hat{\mu}$ and $\hat{\Sigma}$. These are given in Appendix A.1.

3.3. Acquisition functions

A popular acquisition function for deterministic BayesOpt that works well in many scenarios is Expected Improvement (EI). Intuitively, if $f^* = f(\mathbf{x}^*) = \max_{i=1,\ldots,n} f(\mathbf{x}_i)$ is the best value so far observed, then a natural choice of quantity to maximize would be the difference between this and another potential observation $\max\{f(\mathbf{x}) - f^*, 0\}$, which is only non-zero if $f(\mathbf{x}) > f^*$. While the true difference is

https://doi.org/10.1017/dce.2026.10037 Published online by Cambridge University Press

unknown, its expectation under the Gaussian process posterior can be maximized instead: $\alpha_{\mathrm{EI}} = \mathbb{E}[\max\{f(\mathbf{x}) - f^*, 0\}]$. This quantity has a well-known closed-form solution found via integration by parts (Jones et al., 1998)

$$\alpha_{\mathrm{EI}}(\mathbf{x}) = (\mu(\mathbf{x}) - f^*)\Phi(\mathbf{z}) + \sigma(\mathbf{x})\phi(\mathbf{z}) \tag{3.7}$$

where $\mathbf{z} = (\mu(\mathbf{x}) - f^*)/\sigma(\mathbf{x})$, $\Phi(\cdot)$ is the CDF of the standard normal distribution, $\phi(\cdot)$ is the PDF of the standard normal distribution and μ, σ are obtained from the predictive distribution of the surrogate $\hat{f}(\mathbf{x})$. Expected Improvement has the property that its value is high either where there is a good chance of finding a high function value or where the prediction uncertainty is high. A common strategy in the case of constrained optimization is to penalize inputs that are likely to violate the constraints (Schonlau et al., 1998). If the m constraints are assumed to be statistically independent, then the probability that a given $\mathbf{x}$ is feasible under all constraints, that is, $\mathrm{P}[\hat{g}_i(\mathbf{x}) < 0]$, $i = 1, \ldots, m$, given $\hat{g}_i(\mathbf{x}) \sim \mathcal{N}\left(\mu_i(\mathbf{x}), \sigma_i^2(\mathbf{x})\right)$ can be expressed as

$$\alpha_{\mathrm{PF}}(\mathbf{x}) = \prod_{i=1}^{m} \Phi\left(\frac{0 - \mu_i(\mathbf{x})}{\sigma_i(\mathbf{x})}\right), \quad i = 1, \ldots, m \tag{3.8}$$

It is possible to adapt the conventional Expected Improvement acquisition function for the case given by Equation 2.1. Our approach is similar to (Groot et al., 2010), in that we define the Gaussian process model in the joint deterministic-probabilistic $(\mathbf{x}, \boldsymbol{\xi})$ input space and apply results from Bayesian quadrature to integrate out the uncertain parameters. Re-evaluating the acquisition functions above, the Expected Improvement relative to the current maximum $\mu^* = \max_{\mathbf{x}} \mathbb{E}[f(\mathbf{x}, \boldsymbol{\xi})]$ under the Gaussian process posterior is given by

$$\tilde{\alpha}_{\mathrm{EI}}(\mathbf{x}) = (\hat{\mu}(\mathbf{x}) - \mu^*)\Phi(\mathbf{z}) + \hat{\sigma}(\mathbf{x})\phi(\mathbf{z}) \tag{3.9}$$

where $\mathbf{z} = (\hat{\mu}(\mathbf{x}) - \mu^*)/\hat{\sigma}(\mathbf{x})$, and $\hat{\sigma}(\mathbf{x}) = \mathrm{Cov}[f(\mathbf{x}, \boldsymbol{\xi}), f(\mathbf{x}, \boldsymbol{\xi})] = \int \sigma^2(\mathbf{x}, \boldsymbol{\xi}) \mathrm{p}(\boldsymbol{\xi}) d\boldsymbol{\xi}$. The probability a given $\mathbf{x}$ is feasible is similarly given by:

$$\tilde{\alpha}_{\mathrm{PF}}(\mathbf{x}) = \prod_{i=1}^{m} \mathrm{P}[\hat{g}_i(\mathbf{x}, \boldsymbol{\xi}) < 0] = \prod_{i=1}^{m} \int \Phi\left(\frac{0 - \mu_i(\mathbf{x}, \boldsymbol{\xi})}{\sigma_i(\mathbf{x}, \boldsymbol{\xi})}\right) \mathrm{p}(\boldsymbol{\xi}) d\boldsymbol{\xi}, \quad i = 1, \ldots, m \tag{3.10}$$

This BayesOpt strategy selects in each iteration an additional point $\mathbf{x}$ to add to the surrogate via $\mathbf{x}_{\mathrm{new}} := \arg\max_{\mathbf{x}} \tilde{\alpha}_{\mathrm{EI}}(\mathbf{x}) \times \tilde{\alpha}_{\mathrm{PF}}(\mathbf{x})$. Both a new $\mathbf{x}$ and new $\boldsymbol{\xi}$ point are needed, however. Jurecka (2007) suggests a simple approach: selecting $\boldsymbol{\xi}$ based on where both the uncertainty of the Gaussian process model is high and where $\boldsymbol{\xi}$ is likely, as defined by $\mathrm{p}(\boldsymbol{\xi})$. If $\sigma^2(\mathbf{x}, \boldsymbol{\xi})$ is thought of as an estimate for the squared error, weighting it by $\mathrm{p}(\boldsymbol{\xi})$ leads to $\boldsymbol{\xi}_{\mathrm{new}} := \arg\max_{\boldsymbol{\xi}} \alpha_{\mathrm{WSE}}(\mathbf{x}, \boldsymbol{\xi}) := \arg\max_{\boldsymbol{\xi}} \sigma^2(\mathbf{x}, \boldsymbol{\xi}) \mathrm{p}(\boldsymbol{\xi})$.

In comparison with our approach, Toscano-Palmerin and Frazier (2022) optimize $\mathbf{x}$ and $\boldsymbol{\xi}$ jointly, which offers certain advantages. However, these benefits are primarily realized when f varies smoothly and is observed with noise. In our case, f is smooth but observed without noise since the numerical model is deterministic at each $(\mathbf{x}, \boldsymbol{\xi})$. Swersky et al. (2013) select $\boldsymbol{\xi}$ using an expected improvement criterion of $f(\mathbf{x}, \boldsymbol{\xi})$, which does not effectively target the true objective $\mathbb{E}[f(\mathbf{x}, \boldsymbol{\xi})]$. Similarly, Do et al. (2021) define the probability that a candidate $(\mathbf{x}, \boldsymbol{\xi})$ point is feasible using Equation 3.8 rather than Equation 3.10, which does not target the true constraint $\mathrm{P}[g_i(\mathbf{x}, \boldsymbol{\xi}) \leq 0]$.

4. Algorithm

The BayesOpt strategy introduced in Section 3.3 is implemented in Algorithm 1. When optimizing the acquisition functions $\tilde{\alpha}_{\mathrm{EI}}(\mathbf{x}) \times \tilde{\alpha}_{\mathrm{PF}}(\mathbf{x})$ and $\alpha_{\mathrm{WSE}}(\mathbf{x}_{n+1}, \boldsymbol{\xi})$ in Algorithm 1, we use the Adam optimizer from PyTorch in batch mode (Paszke et al., 2019), with Monte Carlo estimates of the integral expression defined by Equations 3.5, 3.6, and 3.10. For example, to compute $\hat{\mu}(\mathbf{x})$, we approximate the integral using Monte Carlo sampling:

https://doi.org/10.1017/dce.2026.10037 Published online by Cambridge University Press

$$\hat{\mu}(\mathbf{x}) = \int \mu(\mathbf{x},\boldsymbol{\xi})\mathrm{p}(\boldsymbol{\xi})d\boldsymbol{\xi} \approx \frac{1}{N}\sum_{i=1}^{N}\mu(\mathbf{x},\boldsymbol{\xi}_i), \quad \boldsymbol{\xi}_i \sim \mathrm{p}(\boldsymbol{\xi}), \tag{4.1}$$

While evaluating the posterior mean at sampled points is inexpensive, Monte Carlo estimates that involve the posterior covariance [of the Gaussian process] can become computationally demanding for large problems due to cubic scaling with the number of samples. Nonetheless, such estimates were found to be sufficient for the purposes of this study. We use the Python package GPyTorch (Gardner et al., 2018), taking advantage of its fast variance predictions (Pleiss et al., 2018) via `gpytorch.settings.fast_pred_var()`. Since $\boldsymbol{\xi}_i$ are fixed once sampled, $\max_{\mathbf{x}} \hat{\mu}(\mathbf{x})$ is a deterministic optimization problem over $\mathbf{x}$, hence gradient-based methods can be applied. PyTorch's automatic differentiation capabilities were used. Analytic expressions are possible for Equations 3.5 and 3.6 when $\mathrm{p}(\boldsymbol{\xi})$ is a normal density (see Appendix A.1), but not for general $\mathrm{p}(\boldsymbol{\xi})$ (Apley et al., 2006; Groot et al., 2010). We note that many uncertainties that influence structures, such as imposed loads, model uncertainties, and sometimes resistance parameters, are non-Gaussian (Vrouwenvelder et al., 1997). Any suitable constrained optimization method can be applied to the constrained problem in the last step of Algorithm 1 $\left(\max_{\mathbf{x}} \mathbb{E}\left[\hat{f}(\mathbf{x},\boldsymbol{\xi})\right] \text{ s.t. } \mathrm{P}[\hat{g}_i(\mathbf{x},\boldsymbol{\xi}) \le 0] \ge 1-\beta_i\right)$.

Efficient initial sampling is implemented where deterministic parameters $\mathbf{x}$ are drawn from bounded uniform distributions $\mathcal{U}[\mathbf{a},\mathbf{b}]$ using Latin Hypercube sampling (scaling uniform samples $\mathbf{u} \in [\mathbf{0},\mathbf{1}]$ via $x_i = a_i + u_i(b_i - a_i)$), while stochastic parameters $\boldsymbol{\xi}$ are generated from a probability distribution $p(\boldsymbol{\xi})$ by creating Latin Hypercube samples $\mathbf{u} \in [\mathbf{0},\mathbf{1}]$ and transforming them via $\boldsymbol{\xi} = F^{-1}(\mathbf{u})$, where F^{-1} is the inverse cumulative distribution function. Training inputs $(\mathbf{x},\boldsymbol{\xi})$ are normalized to the range [0,1], and outputs $y = f(\mathbf{x},\boldsymbol{\xi})$ are standardized (zero mean and unit variance), thereby greatly improving regression stability and performance.

Algorithm 1 BayesOpt for solving reliability-based optimization

1: Evaluate $f(\mathbf{x},\boldsymbol{\xi})$ and $g_i(\mathbf{x},\boldsymbol{\xi})$ for the initial points $\mathcal{D} = \{((\mathbf{x}_i,\boldsymbol{\xi}_i), f(\mathbf{x}_i,\boldsymbol{\xi}_i))\}_{i=1}^{n_0}$.
2: **for** $n = 1$ to N **do**
3: Solve $\mathbf{x}_{n+1} = \arg\max_{\mathbf{x}} \tilde{\alpha}_{\mathrm{EI}}(\mathbf{x}) \times \tilde{\alpha}_{\mathrm{PF}}(\mathbf{x})$.
4: Solve $\boldsymbol{\xi}_{n+1} = \arg\max_{\boldsymbol{\xi}} \alpha_{\mathrm{WSE}}(\mathbf{x}_{n+1},\boldsymbol{\xi})$.
5: Sample $f(\mathbf{x}_{n+1},\boldsymbol{\xi}_{n+1})$ and $g_i(\mathbf{x}_{n+1},\boldsymbol{\xi}_{n+1})$.
6: Update the surrogates $\hat{f}$ and $\hat{g}_i$.
7: **end for**
8: **return** $\mathbf{x}^* = \arg\max_{\mathbf{x}} \mathbb{E}\left[\hat{f}(\mathbf{x},\boldsymbol{\xi})\right]$ **s.t.** $\mathrm{P}[\hat{g}_i(\mathbf{x},\boldsymbol{\xi}) \le 0] \ge 1-\beta_i, \quad i = 1,\ldots,m.$

5. Applications

To graphically illustrate the method set out in Algorithm 1, we use a simple two-dimensional example, given by Equation 5.1 and shown in Figure 2.

$$f(x,\xi) = \frac{\sin(\pi x)}{1 + e^{-10\left(\xi - \frac{1}{2}\right)}} + x^2 - \xi^2 + 10$$

$$g(x,\xi) = -x^2\sin(\xi) - x^3 + \xi^3 - \log\left(1+\xi^2\right) - 1 \tag{5.1}$$

The bounds on the design variable x in this examples are $x \in [0,2]$, and a standard normal distribution is used for the uncertain parameter $\xi \sim \mathcal{N}(0,1)$. The algorithm maximizes $\mathbb{E}[f(\mathbf{x},\boldsymbol{\xi})]$ subject to $\mathrm{P}[g(\mathbf{x},\boldsymbol{\xi}) \le 0] \ge 1 - 0.02$. Figure 2 illustrates the adaptive sampling behavior of the proposed algorithm. Initial points generated via Latin Hypercube sampling cover the space relatively uniformly. The BayesOpt algorithm then strategically adds training points in regions most relevant to the optimization objective: the

https://doi.org/10.1017/dce.2026.10037 Published online by Cambridge University Press

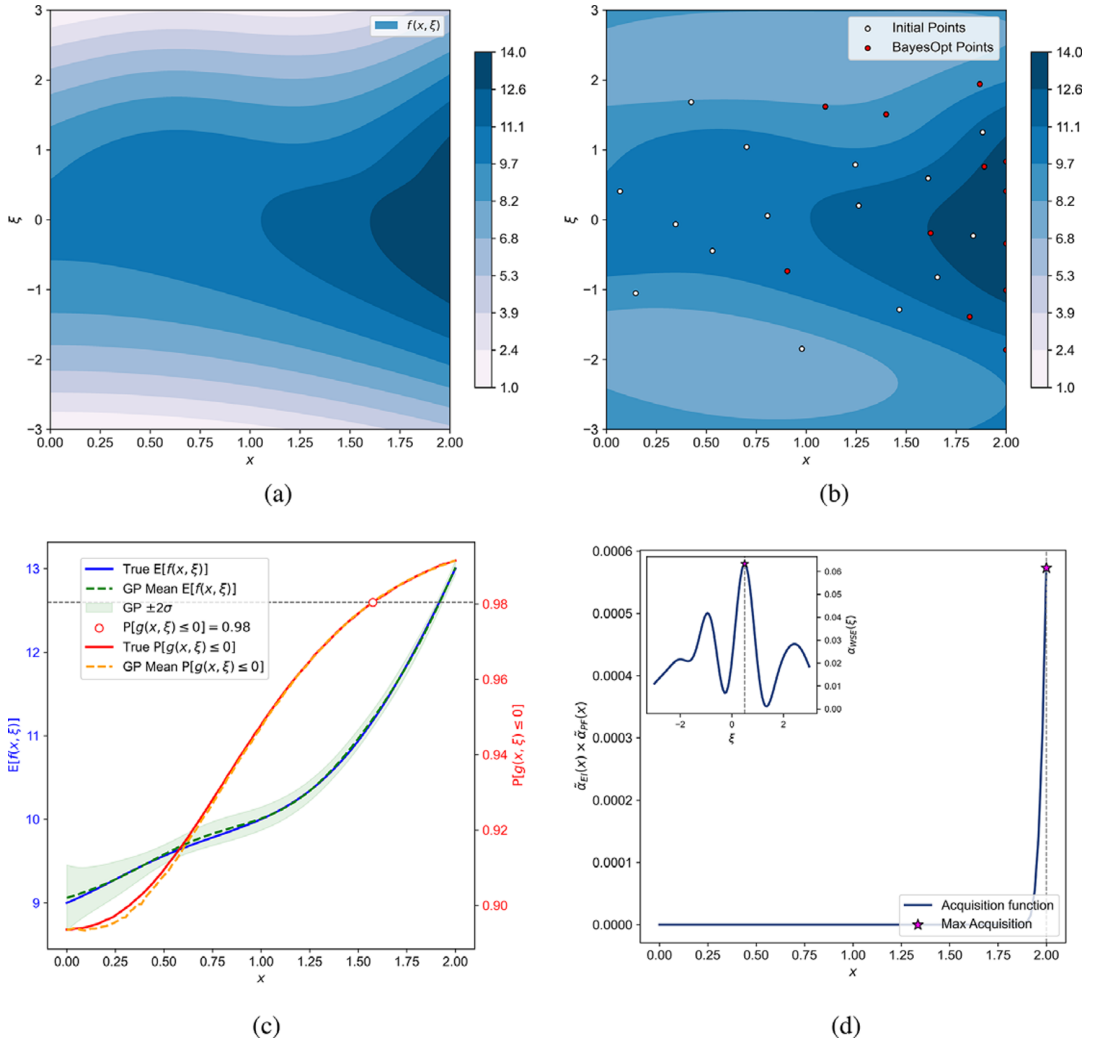


Figure 2. *Visualization of a simple example. (a) true function $f(x,\xi)$, (b) Gaussian process surrogate $\hat{f}(x,\xi)$ with training data plotted, (c) true objective $\mathbb{E}[f(x,\xi)]$ and constraint $\mathrm{P}[g(x,\xi)\leq 0]$ and estimates based on surrogate models $\hat{f}(x,\xi)$ and $\hat{g}(x,\xi)$, (d) acquisition functions $\tilde{\alpha}_{\mathrm{EI}}(x)\times\tilde{\alpha}_{\mathrm{PF}}(x)$ and $\alpha_{\mathrm{WSE}}(\xi)$.*

design space where both $\mathbb{E}[f(\mathbf{x},\boldsymbol{\xi})]$ are high and the reliability constraint $\mathrm{P}[g(\mathbf{x},\boldsymbol{\xi})\leq 0]\geq 1-0.02$ is satisfied (shown by the clustering of BayesOpt points to the right hand side of Figure 2b). Furthermore, new ξ points are sampled where both Gaussian process posterior variance and $p(\boldsymbol{\xi})$ are high (evidenced by the lack of samples at the top and bottom of Figure 2b), since those regions represent low probability (given that ξ is standard normally distributed). The surrogate $\hat{f}(x,\xi)$ in Figure 2b is less accurate away from the selectively sampled BayesOpt points, and hence the estimate $\mathbb{E}[f(x,\xi)]$ in Figure 2c has higher uncertainty closer to $x=0$. This focusing mechanism ensures accurate surrogate approximations where they impact the optimization outcome, while avoiding computational expense in low-value regions of the joint space.

5.1. Branin–Hoo function

Algorithm 1 was applied to a test problem from the literature. Specifically, the Branin–Hoo function described by Williams et al. (2000), modified by the addition of a constraint function, was employed. The

https://doi.org/10.1017/dce.2026.10037 Published online by Cambridge University Press

response function in this case is defined as the product $f(\mathbf{x},\boldsymbol{\xi}) = b(15x_1 - 5, 15\xi_1) \times b(15\xi_2 - 5, 15x_2)$, where b is given by

$$b(u,v) = \left(v - \frac{5.1}{4\pi^2}u^2 + \frac{5}{\pi}u - 6\right)^2 + 10\left(1 - \frac{1}{8\pi}\right)\cos(u) + 10 \tag{5.2}$$

The constraint function is given by $g(\mathbf{x}) = \|\mathbf{x}\|_2 - \sqrt{3/2}$, where $\|\mathbf{x}\|_2$ is the Euclidean norm of the vector $\mathbf{x}$. The design variables are $\mathbf{x} \in [0,1]^2$, and the uncertain parameters $\xi \sim p(\xi)$ are drawn from the probability distribution described in Table 1. The support of the parameter ξ_1 is the set $\Xi_1 = \{0.25, 0.5, 0.75\}$ and for ξ_2, its support is the set $\Xi_1 = \{0.2, 0.4, 0.6, 0.8\}$. The optimization problem is given by the following two finite sums:

$$\mathbb{E}[f(\mathbf{x},\boldsymbol{\xi})] = \sum_{\xi \in \Xi_1 \times \Xi_2} f(x,\xi)p(\xi) \tag{5.3}$$

$$\mathrm{P}[g(\mathbf{x},\boldsymbol{\xi}) \le 0] = \sum_{\zeta \in \Xi_1 \times \Xi_2} p(\xi) \cdot \begin{cases} 1 & \text{if } g(\mathbf{x},\xi) \le 0, \\ 0 & \text{otherwise} \end{cases} \tag{5.4}$$

A contour plot of the objective and constraint is shown in Figure 3. It was found that around 500 training points generated with Latin Hypercube sampling were sufficient to precisely reproduce the true objective and constraint functions. Figure 4 illustrates the convergence performance of the BayesOpt algorithm. Specifically, Figure 4 shows the mean difference between between the true optimum y^* and $\mathbb{E}[f(\mathbf{x}^*,\boldsymbol{\xi})]$ for $x^* = \arg\max \mathbb{E}\left[\hat{f}(\mathbf{x},\boldsymbol{\xi})\right]$ s.t. $\mathrm{P}[\hat{g}_i(\mathbf{x},\boldsymbol{\xi}) \le 0] \ge 1 - \beta_i$ at each iteration, with shaded regions representing two standard deviations of the raw samples. These statistics are calculated directly from the $n = 40$ independent algorithm runs at each iteration, rather than representing a formal confidence interval. The true optimum y^* was found by evaluating a 50×50 grid of evenly spaced design variables $(x_1, x_2 \in [0,1])$, using Monte Carlo sampling with 5000 realizations of the uncertain parameters $\boldsymbol{\xi}$ for each (x_1, x_2) point. The probability $1 - \beta$ was set to 0.9 ($\beta = 0.1$). Two BayesOpt approaches have been investigated. The first, denoted $\alpha_{\mathrm{EI} \times \mathrm{PF}}$, implements an expected improvement acquisition function naively on $f(\mathbf{x},\boldsymbol{\xi})$, that is, uses the update strategy $(\mathbf{x}_{n+1},\boldsymbol{\xi}_{n+1}) = \arg\max_{\mathbf{x}} \alpha_{\mathrm{EI}}(\mathbf{x},\boldsymbol{\xi}) \times \alpha_{\mathrm{PF}}(\mathbf{x},\boldsymbol{\xi})$. The second, denoted $\tilde{\alpha}_{\mathrm{EI} \times \mathrm{PF-WSE}}$ implements Algorithm 1. In the former case, only local information is used at each $(\mathbf{x},\boldsymbol{\xi})$ point, whereas in the latter case, integration is performed over the stochastic parameters. The two approaches are compared to random search, termed $\alpha_{\mathrm{RS}}(x)$.

5.2. Prestressed concrete beam

The BayesOpt algorithm was additionally applied to the design of a prestressed concrete tie-beam (see Figure 5). This example is taken from Burgoyne and Mitchell (2017), who report on the various prestressing systems extant in Coventry Cathedral in the UK. The tie-beam, which is also a pile cap, acts as part of an inverted portal frame to resist the lateral thrust generated at roof level by a shallow-arched shell (Figure 5). Several uncertainties affect this structural system, and to maintain a simple example, we focus specifically on the unknown support stiffnesses provided by the piles—highlighted as influential by the expert review conducted by Burgoyne and Mitchell (2017). Since the system is statically

Table 1. *Joint probability density $p(\xi)$*

$\xi_1\xi_2$	0.2	0.4	0.6	0.8
0.25	0.0375	0.0875	0.0875	0.0375
0.50	0.0750	0.1750	0.1750	0.0750
0.75	0.0375	0.0875	0.0875	0.0375

https://doi.org/10.1017/dce.2026.10037 Published online by Cambridge University Press

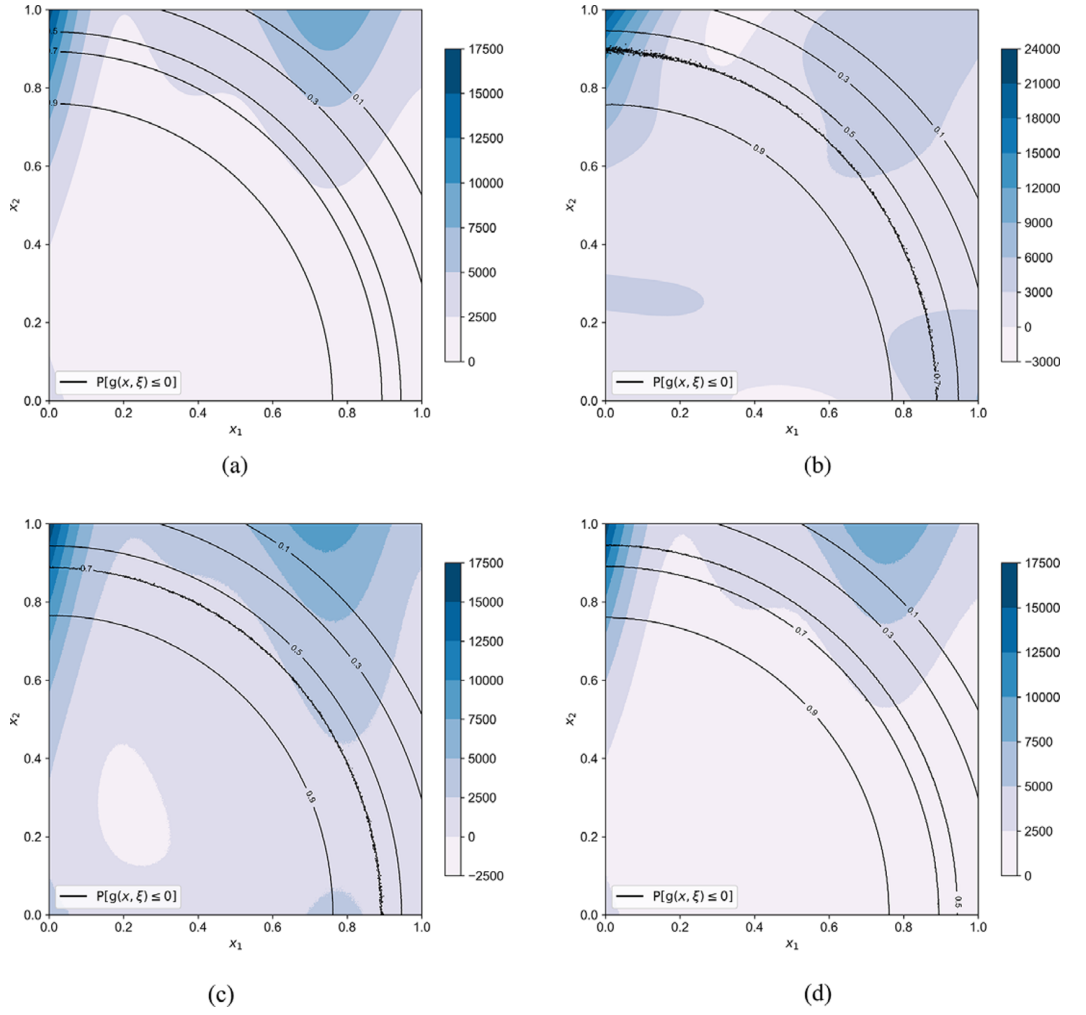


Figure 3. *Shaded contour plots of* $\mathbb{E}[f(\mathbf{x},\boldsymbol{\xi})]$ *for the Branin–Hoo function. Contour lines of the constraint* $\mathrm{P}[g(\mathbf{x},\boldsymbol{\xi})\leq 0]$ *are shown in black. (a) Monte Carlo estimates using 1000* $\boldsymbol{\xi}$ *samples for each point on a 500×500 grid of points (b)* $\mathbb{E}\left[\hat{f}(\mathbf{x},\boldsymbol{\xi})\right]$ *and* $\mathrm{P}[\hat{g}(\mathbf{x},\boldsymbol{\xi})\leq 0]$ *estimated from surrogate models* $\hat{f}$ *and* $\hat{g}$*, each with 100 points, generated with Latin Hypercube sampling, (c) estimates using 250 points, (d) estimates using 500 points.*

indeterminate, the moment distribution in the beam depends on these support stiffnesses, creating uncertainty in the structural response.

The prestress design has been performed in accordance with EN 1992-1-1:2004 (CEN, 2004). A single, straight tendon is assumed at an eccentricity *e*, as shown in Figure 5. Design checks are limited to the serviceability limit state (SLS) for the sake of this study. The ultimate limit states (ULS) typically governs most reinforced concrete designs. However, for prestressed concrete, the amount of prestressing is controlled by the SLS condition, since it is integral to the design philosophy that tensile stress are avoided even under service loads, that is, $f_t = 0$. If the level of prestressing required to satisfy SLS stress constraints proves insufficient to meet ULS requirements, typically additional non-prestressed reinforcing bars are introduced to provide the necessary capacity (The Concrete Society, 2005). The concrete characteristic compressive strength f_{ck} is 50 MPa at service, and 33 MPa at transfer. Short- and long-term

https://doi.org/10.1017/dce.2026.10037 Published online by Cambridge University Press

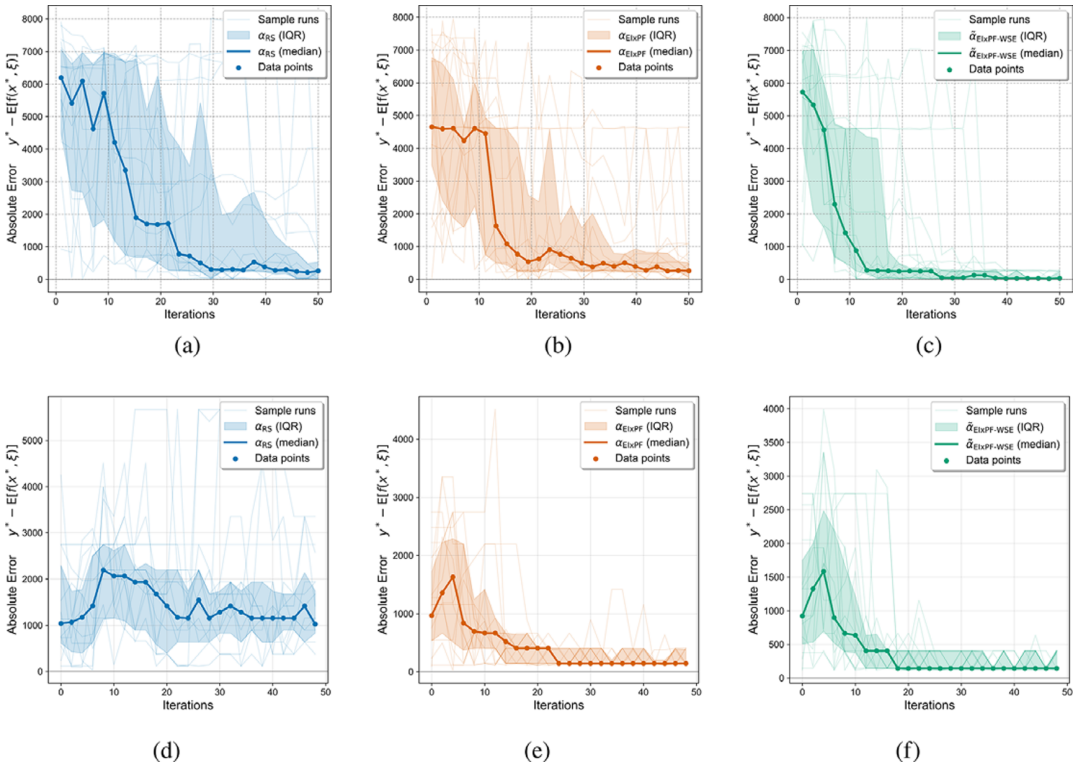


Figure 4. *BayesOpt results for constrained Branin–Hoo example (a–c) and prestressed beam example (d–f). (a,d) optimization using random search* $(\mathbf{x}_{n+1}, \boldsymbol{\xi}_{n+1}) \sim \mathcal{U}[\mathcal{X} \times \Xi]$*, (b,e) optimization using conventional Expected Improvement* $(\mathbf{x}_{n+1}, \boldsymbol{\xi}_{n+1}) = \arg\max_{\mathbf{x}} \alpha_{\mathrm{EI}}(\mathbf{x}, \boldsymbol{\xi}) \times \alpha_{\mathrm{PF}}(\mathbf{x}, \boldsymbol{\xi})$*, (c,f) optimization using Algorithm 1. The three algorithms were each run 40 times.*

loading here relates to forces (1) at the transfer of prestress forces to the beam, where the prestress force and the self-weight must be considered, and (2) when the beam is under the influence of all of the applied loads. To avoid cracking and excessive levels of creep, compressive stress in the concrete should be limited to $f_c = 0.6\, f_{ck}$. The steel tendons have characteristic and design strengths of $f_{pk} = 1860$ MPa and $f_{p,\max} = 0.8\, f_{pk}$ respectively. The Young's modulus E of the concrete is 30 GPa. The densities of concrete and steel are 24 kN/m^3 and 78.5 kN/m^3, respectively.

Instantaneous and time-dependent prestress losses are considered for cases one and two, respectively. Initial prestress losses due to elastic shortening, friction, and wedge draw-in of the anchorage are estimated as five percent of the initial prestress force, whilst time-dependent losses due to creep and shrinkage are estimated as ten percent of the initial prestress force. These values lie within the typical range of losses encountered in design (Utrilla and Samartín, 1997).

The requirement for the stress limits $-f_c \le \sigma \le f_t$ to hold at both the top and bottom fiber of the beam cross-section, at both the transfer and service states, for both hogging and sagging beam moments, can be summarized by the following eight equations (see Appendix A.2):

$$g_1 = \frac{\eta_0 P}{A} + \frac{M_{\mathrm{hog},0}}{Z} - f_{t,0}, \quad g_2 = -\left(\frac{\eta_0 P}{A} - \frac{M_{\mathrm{hog},0}}{Z}\right) - f_{c,0} \tag{5.5}$$

$$g_3 = \frac{\eta_0 P}{A} - \frac{M_{\mathrm{sag},0}}{Z} - f_{t,0}, \quad g_4 = -\left(\frac{\eta_0 P}{A} + \frac{M_{\mathrm{sag},0}}{Z}\right) - f_{c,0} \tag{5.6}$$

https://doi.org/10.1017/dce.2026.10037 Published online by Cambridge University Press

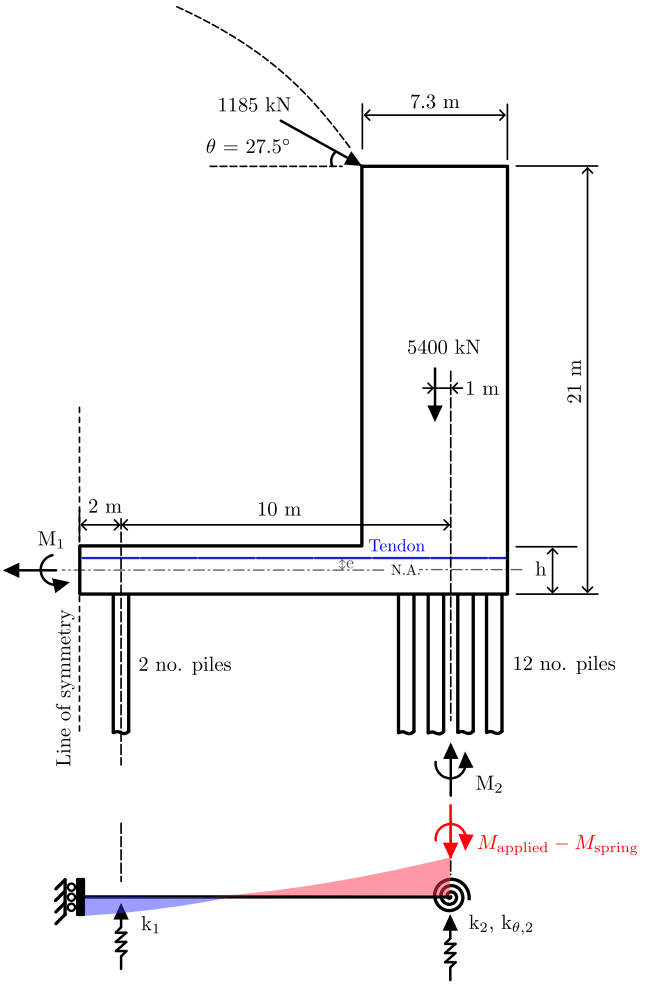


Figure 5. *Prestressed tie beam (adapted from Burgoyne and Mitchell, 2017).*

$$g_5 = \frac{\eta_1 P}{A} + \frac{M_{\text{hog},1}}{Z} - f_{t,1}, \quad g_6 = -\left(\frac{\eta_1 P}{A} - \frac{M_{\text{hog},1}}{Z}\right) - f_{c,1} \tag{5.7}$$

$$g_7 = \frac{\eta_1 P}{A} - \frac{M_{\text{sag},1}}{Z} - f_{t,1}, \quad g_8 = -\left(\frac{\eta_1 P}{A} + \frac{M_{\text{sag},1}}{Z}\right) - f_{c,1} \tag{5.8}$$

where Z is the section modulus, which is equal above and below the neutral axis since a rectangular cross-section is used. Subcscripts 0 and 1 refer to the transfer and service states. The term η accounts for the prestress losses, that is, $\eta_0 = 0.95$ at transfer and $\eta_1 = 0.9$ in service. To handle the statistical indeterminacy of this example, the effects due to prestress eccentricity (Pe) are incorporated as applied moments in the structural analysis model (see Appendix A.3), and the maximum hogging M_{hog} and sagging M_{sag} moments in the beam are computed accordingly. These moments then only need to be combined with the term P/A to compute the limit state equations $g_i \leq 0$, $i = 1, 2, \ldots, 8$. The self-weight is included in the model. Compression is taken negative, as are sagging bending moments. Figure 6 visualizes the limit state functions for this example. The objective in this case (which can be negated to get minimum cost) is deterministic and given by

https://doi.org/10.1017/dce.2026.10037 Published online by Cambridge University Press

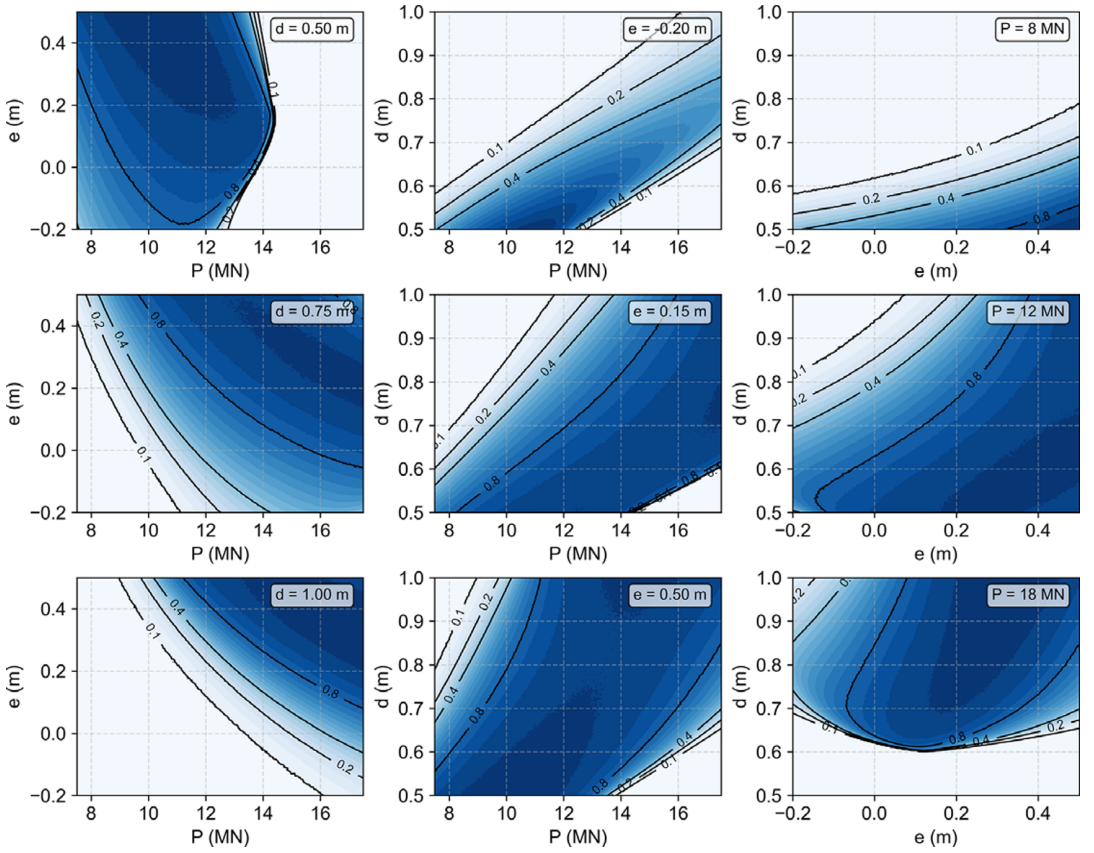


Figure 6. *Two-dimensional cross-sections through the three-dimensional parameter space (P, e, d), with contour lines showing probability levels* $\prod_i \mathrm{P}[g_i(\mathbf{x},\boldsymbol{\xi}) \le 0] = (0.1, 0.2, 0.4, 0.8)$ *The contours were generated via Monte Carlo sampling of surrogates on a 200x200 grid using 5000* $\boldsymbol{\xi}$ *samples per point.*

$$\mathbb{E}[f(\mathbf{x})] = \mathrm{cost}(\mathbf{x}) = V_c(\mathbf{x})c_c + M_s(\mathbf{x})c_s + A_f(\mathbf{x})c_f \tag{5.9}$$

The design variables $\mathbf{x} = [P, e, d]$ are the beam prestress force (in MN), eccentricity above the neutral axis (in m), and cross-section depth (in m). The bounds on these variables are: $P \in [2, 15]$, $e \in [-0.45, 0.45]$, and $d \in [0.5, 1.5]$. The beam width was fixed at $b = 1.5$ m. The uncertain parameters are $\boldsymbol{\xi} = [k_A, k_B]$, which represent nominal stiffnesses (in kN/mm) used to compute the linear and rotational support stiffnesses included in the beam model visualized in Figure 5; specifically, the following relationships are used: $k_1 = (0.7 \times 2) \cdot k_A, k_2 = (0.7 \times 12) \cdot k_B, k_{2,\theta} = (0.7 \times 60) \cdot k_B$, assuming an efficiency factor of 0.7 for the pile groups. The symbols c_c, c_s, and c_f represent cost coefficients for the concrete, prestressing tendons, and formwork, respectively. The following numerical values were used: $c_c = 145\ £/m^3$, $c_s = 6000\ £/\text{tonne}$ and $c_f = 36\ £/m^2$. These coefficients operate on the volume of concrete $V_c = bhL$, the beam side area $A_f = 2dL$, and the mass of steel tendons required $M_s = \rho_s LP/f_{p,\max}$, as defined by Equation 5.9. The uncertainties were assumed multivariate normal, $\boldsymbol{\xi} \sim \mathcal{N}(\boldsymbol{\mu}_\xi, \Sigma_\xi)$, with mean vector $\boldsymbol{\mu}_\xi = [100\ 100]^T$ kN/mm and covariance matrix:

$$\Sigma_\xi = \begin{bmatrix} 30^2 & 0.5(30)^2 \\ 0.5(30)^2 & 30^2 \end{bmatrix} \tag{5.10}$$

https://doi.org/10.1017/dce.2026.10037 Published online by Cambridge University Press

A coefficient of variation of 30% indicates that the random variables k_A and k_B have a standard deviation of 30 kN/mm. This represents a medium-to-high estimate for inherent soil property variation (Phoon and Kulhawy, 1999). The correlation coefficient of 0.5 avoids the unrealistic assumptions of perfect correlation or complete independence between nearby pile groups, reflecting that both are influenced by similar ground conditions. Both the coefficient of variation and correlation parameters can be refined based on site-specific ground investigation data. The probability $1-\beta_i$ was set to 0.99 for all constraints ($\beta_i = 0.01$). For reference, the Eurocode target reliability index prescribed for a 50-year reference period for SLS design is $\beta = 1.5$, which corresponds to a failure probability $P_f \approx 0.07$. Figure 4 shows the BayesOpt results for the prestressed concrete example. The optimal solution, found by evaluating a 20×20×20 grid of evenly spaced design variables $[P, e, d]$ (using Monte Carlo sampling with 1000 realizations of the uncertain parameters $\boldsymbol{\xi}$), is $\mathbf{x}^* = (10.13,\ 0.45,\ 0.5)$, with optimal cost $y^* = £5,584$. A surrogate model trained on a large number of points was used to plot Figure 6 (as discussed in Section 5.4), although the true numerical model was used when locating the optimal point $\mathbf{x}^*$.

5.3. Comparison of algorithm performance

For the Branin–Hoo function example, only Algorithm 1 converges to the correct solution (see Figure 4c), correctly predicting the true optimum over almost all runs of the algorithm. The approach using $\alpha_{\mathrm{EI}\times\mathrm{PF}}$ shows an improved performance over random search, with a similar median trend between Figure 4a and Figure 4b but tighter interquartile range for the $\alpha_{\mathrm{EI}\times\mathrm{PF}}$ strategy. This improvement over random search is likely due to there being some similarity between $f(\mathbf{x},\boldsymbol{\xi})$ and $\mathbb{E}[f\mathbf{x},\boldsymbol{\xi}]$ and the Gaussian process point estimate probability for $g(\mathbf{x},\boldsymbol{\xi}) \leq 0$ being similar to $\mathrm{P}[g(\mathbf{x},\boldsymbol{\xi}) < 0]$. Hence, the same principles which allow Algorithm 1 to perform well also partially apply to the approach utilizing $\alpha_{\mathrm{EI}\times\mathrm{PF}}$.

The prestressed beam problem shows a somewhat similar trend in algorithm performance; random search struggles to consistently identify the correct solution, the approach using $\alpha_{\mathrm{EI}\times\mathrm{PF}}$ shows improved consistency, as does Algorithm 1 in targeting the true optimum. The two test problems present different challenges: the Branin–Hoo function features multiple local optima but a relatively simple constraint boundary, while the prestressed beam problem has a more complex feasible region and a simple linear objective function. Algorithm 1 demonstrates robust performance across both problem types, maintaining consistent convergence behavior and solution quality. In contrast, random search in particular shows performance degradation when moving from the Branin–Hoo function to the prestressed beam problem.

5.4. Prestressed beam design and surrogate modeling

Surrogate modeling of the prestressed beam optimization problem requires careful consideration due to the relationship between design variables, uncertain parameters, and structural responses. The constraint functions $g_i(\mathbf{x},\boldsymbol{\xi})$ depend on maximum beam moments computed from structural analysis, where the $\max(\cdot)$ operator could potentially introduce non-smoothness. Discontinuous and non-smooth behavior violates the assumptions involved in Gaussian process regression. However, we found that the maximum moments vary smoothly enough with the design parameters $\mathbf{x} = [P, e, d]$ that the resulting constraint surfaces remain well-behaved for Gaussian process modeling. This requirement for smooth and continuous limit state functions is also in a sense a limitation of the proposed method, as non-smooth nonlinear analysis programs may struggle to be modeled in a data-efficient way by Gaussian process surrogates.

For the Bayesian optimization results in this study, standard Gaussian processes were used as surrogates for both the objective and constraints. However, for visualization of the reliability contours shown in Figure 6, scalable variational Gaussian processes, as expounded upon in Appendix A.4, were employed to ensure an accurate representation of the constraint probability surfaces. Scalable Gaussian processes facilitate the use of larger training datasets. Each surrogate used to create Figure 6 was trained on 2000 points.

In this study, the practical integration of BayesOpt and reliability analysis within engineering design has been illustrated through a simplified prestressed concrete example. Comprehensive prestressed concrete design encompasses numerous additional checks that warrant incorporation into future optimization frameworks: additional considerations exist at the system level, such as the optimization of

https://doi.org/10.1017/dce.2026.10037 Published online by Cambridge University Press

prestressing sequences in multi-tendon systems [to minimize elastic shortening losses]; ULS and SLS verification as mandated by Eurocode 2 (including ultimate moment and shear capacity), deflection limits, and crack width control. Further considerations exists, such as tendon profile geometry, duct spacing, and grouting access. It is likely the structural design of the tie-beam example could be made more efficient if a draped tendon profile were used in place of a straight cable. It would need to be verified, however, that the moment envelope is suitably consistent given the uncertainties present in the design.

Beyond the ground stiffness uncertainties addressed in this work, a more comprehensive reliability analysis could incorporate additional sources of variability, including material property variations in concrete and prestressing steel strengths, geometric tolerances, construction quality factors, and loading uncertainties. Environmental conditions affecting long-term prestress losses, such as humidity and temperature variations, introduce further uncertainty that could also impact the selection of appropriate probabilistic models for the resistance parameters. Future extensions of this optimization framework could address these limitations through expanded constraint sets, the incorporation of additional uncertain parameters, and the development of multi-objective formulations that balance initial construction costs against life-cycle performance and structural robustness.

6. Conclusion

This paper presents a reliability-constrained Bayesian optimization framework for structural design under uncertainty. Our approach efficiently manages uncertainties from arbitrary probability distributions while leveraging gradient-based optimization for acquisition function maximization. Through the Branin–Hoo function and prestressed tie-beam examples, we demonstrated that the proposed approach, which integrates uncertainty in both objective function and constraints, performs well in terms of convergence rate and solution quality.

While our test problems involve only a small number of design variables and uncertain parameters, the methods could extend to larger-scale engineering problems through adaptive sampling strategies or dimension reduction techniques. Future research could explore larger real-world structural examples using expensive finite-element analysis and multi-objective optimization approaches. The use of high-fidelity simulations would introduce additional practical challenges, such as numerical noise from iterative solvers, high-dimensional design spaces, and a greater impetus for parallelization of numerical models.

Data availability statement. The code and synthetic data used to support the findings in this study can be found at: https://doi.org/10.5281/zenodo.17974903 (Whiteley and Becque, 2025).

Acknowledgements. The authors would like to thank Laing O'Rourke Ltd for offering valuable insight throughout the course of the project.

Author contribution. Conceptualization-Equal: J.W., J.B.; Data Curation-Lead: J.W.; Formal Analysis-Lead: J.W.; Funding Acquisition-Equal: J.B.; Funding Acquisition-Lead: J.B.; Investigation-Equal: J.W., J.B.; Methodology-Equal: J.W., J.B.; Methodology-Lead: J.W.; Project Administration-Equal: J.W., J.B.; Software-Equal: J.W.; Software-Lead: J.W.; Validation-Equal: J.W., J.B.; Visualization-Equal: J.W.; Visualisation-Lead: J.W.; Writing–Original Draft-Equal: J.W.; Writing-Original Draft-Lead: J.W.; Writing–Review & Editing-Equal: J.W., J.B.

Funding statement. The authors gratefully acknowledge the EPSRC and Laing O'Rourke Ltd for funding this research through the EPSRC Centre for Doctoral Training in Future Infrastructure and Built Environment: Resilience in a Changing World, under grant number EP/S02302X/1.

Competing interests. The authors declare none.

References

Apley DW, **Liu J and Chen W** (2006) Understanding the effects of model uncertainty in robust design with computer experiments. *Journal of Mechanical Design 128*(4), 945–958.

Arendt PD, **Apley DW and Chen W** (2013) Objective-oriented sequential sampling for simulation based robust design considering multiple sources of uncertainty. *Journal of Mechanical Design 135*(5), 051005.

Bichon BJ, **Eldred MS**, **Swiler LP**, **Mahadevan S and McFarland JM** (2008) Efficient global reliability analysis for nonlinear implicit performance functions. *AIAA Journal 46*(10), 2459–2468.

Burgoyne C and Mitchell O (2017) Prestressing in Coventry *cathedral*. *Structure 11*, 62–83.

Campi MC and Garatti S (2011) A sampling-and-discarding approach to chance-constrained optimization: Feasibility and optimality. *Journal of Optimization Theory and Applications 148*(2), 257–280.

CEN. (2002). EN 1990: Eurocode: Basis of structural design.

CEN. (2004). EN 1991-1-1: Eurocode 2: Design of concrete structures - General rules and rules for buildings.

Daulton S, **Cakmak S**, **Balandat M**, **Osborne MA**, **Zhou E and Bakshy E** (2022) Robust multi-objective bayesian optimization under input noise. In *Proceedings of the 39th International Conference on Machine Learning*. PMLR, Vol. *162*, pp. 4831–4866.

Do B, **Ohsaki M and Yamakawa M** (2021) Bayesian optimization for robust design of steel frames with joint and individual probabilistic constraints. *Engineering Structures 245*, 112859.

Ellingwood B, **MacGregor JG**, **Galambos TV and Cornell CA** (1982) Probability based load criteria: Load factors and load combinations. *Journal of the Structural Division 108*(5), 978–997.

Faber MH and Sørensen JD (2002) *Reliability Based Code Calibration*. Zurich, Switzerland: The Joint Committee on Structural Safety

Frazier PI (2018) Bayesian optimization. In *INFORMS Tutorials in Operations Research*, pp. 255–278. https://doi.org/10.1287/educ.2018.0188.

Gardner J, **Pleiss G**, **Weinberger KQ**, **Bindel D and Wilson AG** (2018) Gpytorch: Black-box matrix-matrix gaussian process inference with gpu acceleration. *Advances in Neural Information Processing Systems 31*.

Groot P, **Birlutiu A and Heskes T** (2010) Bayesian Monte Carlo for the global optimization of expensive functions. In Coelho H, Studer R and Wooldridg M (eds.), *Proceedings of the 2010 Conference on ECAI 2010: 19th European Conference on Artificial Intelligence*. IOS Press. https://doi.org/10.3233/978-1-60750-606-5-249.

Hilton HH and Feigen M (1960) Minimum weight analysis based on structural reliability. *Journal of the Aerospace Sciences 27*(9), 641–652.

Hu W, **Cheng S**, **Yan J**, **Cheng J**, **Peng X**, **Cho H and Lee I** (2024) Reliability-based design optimization: A state-of-the-art review of its methodologies, applications, and challenges. *Structural and Multidisciplinary Optimization 67*(9), 168.

Jones DR, **Schonlau M and Welch WJ** (1998) Efficient global optimization of expensive black-box functions. *Journal of Global Optimization 13*, 455–492.

Jurecka F (2007) *Robust Design Optimization Based on Metamodeling Techniques*. München: Doctoral dissertation, Technische Universität

Khachiyan LG (1989) The problem of calculating the volume of a polyhedron is enumerably hard. *Russian Mathematical Surveys 44*(3), 199.

Mathern A, **Steinholtz OS**, **Sjöberg A**, **Önnheim M**, **Ek K**, **Rempling R**, **Gustavsson E and Jirstrand M** (2021) Multi-objective constrained bayesian optimization for structural design. *Structural and Multidisciplinary Optimization 63*(2), 689–701.

Moustapha M and Sudret B (2019) Surrogate-assisted reliability-based design optimization: A survey and a unified modular framework. *Structural and Multidisciplinary Optimization 60*(5), 2157–2176.

O'Hagan A (1991) Bayes–hermite quadrature. *Journal of Statistical Planning and Inference 29*(3), 245–260.

Paszke A, **Gross S**, **Massa F**, **Lerer A**, **Bradbury J**, **Chanan G**, **Killeen T**, **Lin Z**, **Gimelshein N**, **Antiga L**, *et al.* (2019) Pytorch: An imperative style, high-performance deep learning library. *Advances in Neural Information Processing Systems* 32.

Phoon K-K and Kulhawy FH (1999) Characterization of geotechnical variability. *Canadian Geotechnical Journal 36*(4), 612–624.

Pleiss G, **Gardner J**, **Weinberger K and Wilson AG** (2018) Constant-time predictive distributions for gaussian processes. In *Proceedings of the 35th International Conference on Machine Learning*. PMLR, Vol. *80*, pp. 4114–4123.

Przemieniecki JS (1985) *Theory of Matrix Structural Analysis*. Mineola, NY: Dover Publications Inc.

Rasmussen CE and Ghahramani Z (2003) Bayesian Monte Carlo. *Advances in Neural Information Processing Systems 15*.

Rasmussen CE and Williams CKI (2006) *Gaussian Processes for Machine Learning*. Cambridge, MA: The MIT Press.

Schonlau M, **Welch WJ and Jones DR** (1998) Global versus local search in constrained optimization of computer models. *Lecture notes-monograph series 34*, 11–25.

Sui Y, **Gotovos A**, **Burdick J and Krause A** (2015) Safe exploration for optimization with gaussian processes. In *Proceedings of the 32nd International Conference on Machine Learning*. PMLR, Vol. *37*, pp. 997–1005.

Swersky K, **Snoek J and Adams RP** (2013) Multi-task bayesian optimization. *Advances in Neural Information Processing Systems 26*.

Tesch M, **Schneider J and Choset H** (2011) Adapting control policies for expensive systems to changing environments. In *2011 IEEE/RSJ International Conference on Intelligent Robots and Systems*. IEEE, pp. 357–364.

The Concrete Society (2005) Post-tensioned concrete floors: Design handbook. *Concrete Society Technical Report 43*.

Toscano-Palmerin S and Frazier PI (2022) Bayesian optimization with expensive integrands. *SIAM Journal on Optimization 32*(2), 417–444.

Utrilla M and Samartín A (1997) Optimized design of the prestress in continuous bridge decks. *Computers & Structures 64*(1-4), 719–728.

Vrouwenvelder T, *et al.* (1997) The JCSS probabilistic model code. *Structural Safety 19*(3), 245–251.

https://doi.org/10.1017/dce.2026.10037 Published online by Cambridge University Press

Whiteley J and Becque J (2025) *Replication data for: A Bayesian optimization approach for reliability-based design of prestressed concrete structures.* https://doi.org/10.5281/zenodo.17974903.

Williams BJ, **Santner TJ and Notz WI** (2000) Sequential design of computer experiments to minimize integrated response functions. *Statistica Sinica 10*, 1133–1152.

Zhang S, **Zhu P**, **Chen W and Arendt P** (2013) Concurrent treatment of parametric uncertainty and metamodeling uncertainty in robust design. *Structural and Multidisciplinary Optimization 47*, 63–76.

A. Appendices

A.1. Bayes–Hermite quadrature

The squared exponential kernel in the joint space $\left(\mathbf{x}\in\mathbb{R}^{d_x},\boldsymbol{\xi}\in\mathbb{R}^{d_\xi}\right)$, with ℓ hyperparameter unique to each dimension, is separable, that is, $k((\mathbf{x},\boldsymbol{\xi}),(\mathbf{x}',\boldsymbol{\xi}'))=\sigma_f^2 k_x(\mathbf{x},\mathbf{x}')k_\xi(\boldsymbol{\xi},\boldsymbol{\xi}')$, with

$$k_x(\mathbf{x},\mathbf{x}')=\exp\left(-\frac{1}{2}(\mathbf{x}-\mathbf{x}')^\top A_x^{-1}(\mathbf{x}-\mathbf{x}')\right)\text{ and }k_\xi(\boldsymbol{\xi},\boldsymbol{\xi}')=\exp\left(-\frac{1}{2}(\boldsymbol{\xi}-\boldsymbol{\xi}')^\top A_\xi^{-1}(\boldsymbol{\xi}-\boldsymbol{\xi}')\right)\tag{A.1}$$

where $A_x=\operatorname{diag}\left(\ell_{x,1}^2,\ldots,\ell_{x,d_x}^2\right)$ and $A_\xi=\operatorname{diag}\left(\ell_{\xi,1}^2,\ldots,\ell_{\xi,d_\xi}^2\right)$. If the uncertain parameters in the expression $\overline{f}(\mathbf{x})=\int\hat{f}(\mathbf{x},\boldsymbol{\xi})p(\boldsymbol{\xi})d\boldsymbol{\xi}$ are jointly Gaussian, $p(\boldsymbol{\xi})=\mathcal{N}\left(\boldsymbol{\mu}_\xi,\boldsymbol{\Sigma}_\xi\right)$, and observations are noiseless, then the distribution $p\left(\overline{f}|\mathcal{D}\right)$ is Gaussian with mean and covariance (Rasmussen and Ghahramani, 2003):

$$\mathbb{E}_{f|\mathcal{D}}\left[\overline{f}(\mathbf{x})\right]=\mathbf{w}(\mathbf{x})^\top K^{-1}\mathbf{y}\tag{A.2}$$

$$\operatorname{Cov}_{f|\mathcal{D}}\left[\overline{f}(\mathbf{x}),\overline{f}(\mathbf{x}')\right]=\sigma_f^2 k_x(\mathbf{x},\mathbf{x}')\left|2A_\xi^{-1}\Sigma_\xi+I_{d_\xi}\right|^{-1/2}-\mathbf{w}(\mathbf{x})^\top K^{-1}\mathbf{w}(\mathbf{x}')\tag{A.3}$$

where

$$\mathbf{w}(\mathbf{x})=\left[\sigma_f^2 k_x(\mathbf{x},\mathbf{x}_i)\left|A_\xi^{-1}\Sigma_\xi+I_{d_\xi}\right|^{-1/2}\exp\left(-\frac{1}{2}\left(\boldsymbol{\xi}_i-\boldsymbol{\mu}_\xi\right)^\top\left(A_\xi+\Sigma_\xi\right)^{-1}\left(\boldsymbol{\xi}_i-\boldsymbol{\mu}_\xi\right)\right)\right]_{i=1}^{n}\tag{A.4}$$

A.2. Prestress design

Considering only one loading scenario (the forces on the beam at the transfer of prestress—no forces are applied to the structure other than prestress and self-weight), there exist maximum hogging and sagging moments in the beam: $M_{\text{hog}}\geq 0$ and $M_{\text{sag}}\leq 0$. The stresses at the top and bottom fibers of the beam are:

$$\sigma_{\text{top}}=\frac{P}{A}+\frac{M}{Z}\tag{A.5}$$

$$\sigma_{\text{bottom}}=\frac{P}{A}-\frac{M}{Z}\tag{A.6}$$

where M includes the prestressing moment Pe. Note that in statically indeterminate structures, the prestressing force induces secondary moments due to the restraint of deformations at the supports; M represents the total moment including both primary (Pe) and secondary effects. At each fiber, the stress must satisfy $-f_c\leq\sigma\leq f_t$. This leads to the following eight inequalities:

$$h_1:\frac{P}{A}+\frac{M_{\text{hog}}}{Z}\geq -f_c,\quad h_5:\frac{P}{A}+\frac{M_{\text{sag}}}{Z}\geq -f_c\tag{A.7}$$

$$h_2:\frac{P}{A}+\frac{M_{\text{hog}}}{Z}\leq f_t,\quad h_6:\frac{P}{A}+\frac{M_{\text{sag}}}{Z}\leq f_t\tag{A.8}$$

$$h_3:\frac{P}{A}-\frac{M_{\text{hog}}}{Z}\geq -f_c,\quad h_7:\frac{P}{A}-\frac{M_{\text{sag}}}{Z}\geq -f_c\tag{A.9}$$

$$h_4:\frac{P}{A}-\frac{M_{\text{hog}}}{Z}\leq f_t,\quad h_8:\frac{P}{A}-\frac{M_{\text{sag}}}{Z}\leq f_t\tag{A.10}$$

Given that $P\leq 0$ (compression), $M_{\text{hog}}\geq 0$, $M_{\text{sag}}\leq 0$, and that the beam is rectangular $\left(Z_{\text{top}}=Z_{\text{bottom}}=Z\right)$, several of these constraints will never govern. For instance, h_1 is redundant because if h_3 is satisfied, then h_1 is automatically satisfied. Similarly, h_7 is redundant when h_5 is satisfied, h_4 is redundant when h_2 is satisfied, and h_6 is redundant when h_8 is satisfied. The non-redundant equations, written as limit states $g_i\leq 0$, correspond to exceeding either the tensile or compressive stress limits, and can be written as:

$$g_1=\frac{P}{A}+\frac{M_{\text{hog}}}{Z}-f_t,\quad g_2=-\left(\frac{P}{A}-\frac{M_{\text{hog}}}{Z}\right)-f_c\tag{A.11}$$

$$g_3=\frac{P}{A}-\frac{M_{\text{sag}}}{Z}-f_t,\quad g_4=-\left(\frac{P}{A}+\frac{M_{\text{sag}}}{Z}\right)-f_c\tag{A.12}$$

https://doi.org/10.1017/dce.2026.10037 Published online by Cambridge University Press

A.3. Direct stiffness method

The direct stiffness method utilizes the local element-level force-displacement relationship $\mathbf{f} = \mathbf{k}\mathbf{u}$. In the general case, $\mathbf{f}_\mathrm{i} = \begin{bmatrix} f_{xi} & f_{yi} & f_{zi} & m_{xi} & m_{yi} & m_{zi} \end{bmatrix}^\mathrm{T}$ contains the member forces and moments at one end node and $\mathbf{u}_\mathrm{i} = \begin{bmatrix} u_{xi} & u_{yi} & u_{zi} & \theta_{xi} & \theta_{yi} & \theta_{zi} \end{bmatrix}^\mathrm{T}$ contains the corresponding displacements and rotations. Displacements and rotations are assumed to be small. We then define:

$$\mathbf{f} = \begin{bmatrix} f_1 \\ f_2 \end{bmatrix}, \quad \mathbf{u} = \begin{bmatrix} u_1 \\ u_2 \end{bmatrix} \tag{A.13}$$

where the indices 1 and 2 refer to the end nodes of the element. The local stiffness matrix $\mathbf{k}$ is the standard element stiffness matrix for Euler-Bernoulli beam elements considering axial and flexural deformations but neglecting shear deformations (Przemieniecki, 1985). The global force-displacement relation in global coordinates, considering all elements ($\mathrm{e} = 1, 2, \ldots, \mathrm{N}$) in the system, is $\mathbf{K}^*\mathbf{u}^* = \mathbf{f}^*$, with.

$$\mathbf{K}^* = \sum_{\mathrm{e}=1}^{\mathrm{N}} \left(\mathbf{T}^\mathrm{T}\mathbf{k}\mathbf{T}\right)_e \tag{A.14}$$

When assembling the global matrix $\mathbf{K}^*$, each element's contributions are mapped from local to global degrees of freedom in the conventional way. The transformation matrix $\mathbf{T}$ contains direction cosines, mapping the local coordinate basis aligned with the element axis to global Cartesian coordinates. The system can be partitioned based on the sets of free ($\mathcal{F}$) and constrained (C) degrees of freedom.

$$\mathbf{K}^* = \begin{bmatrix} \mathbf{K}_{\mathcal{F}\mathcal{F}} & \mathbf{K}_{\mathcal{F}C} \\ \mathbf{K}_{C\mathcal{F}} & \mathbf{K}_{CC} \end{bmatrix}, \quad \mathbf{f}^* = \begin{bmatrix} \mathbf{f}_\mathcal{F} \\ \mathbf{f}_C \end{bmatrix}, \quad \mathbf{u}^* = \begin{bmatrix} \mathbf{u}_\mathcal{F} \\ \mathbf{u}_C \end{bmatrix} \tag{A.15}$$

In the case of elastic supports, finite stiffness values (k_i for translation and $k_{\theta,i}$ for rotation) are indexed into $\mathbf{K}_{\mathcal{F}\mathcal{F}}$, with their positions corresponding to the relevant degrees of freedom. For rigid supports, displacements at the constrained degrees of freedom are set to zero ($\mathbf{u}_C = 0$) and the system reduces to:

$$\mathbf{K}_{\mathcal{F}\mathcal{F}}\,\mathbf{u}_\mathcal{F} = \mathbf{f}_\mathcal{F} \quad \Rightarrow \quad \mathbf{u}_\mathcal{F} = \mathbf{K}_{\mathcal{F}\mathcal{F}}^{-1}\,\mathbf{f}_\mathcal{F} \tag{A.16}$$

The reaction forces at the constrained degrees of freedom are then computed as $\mathbf{f}_C = \mathbf{K}_{C\mathcal{F}}\,\mathbf{u}_\mathcal{F}$ and internal member forces can be interpolated from nodal values.

A.4. Variational Gaussian process

A Variational Gaussian process provides a scalable approximation to exact Gaussian process inference using sparse variational techniques. In this work, we use a standard regression model:

$$y = f(\mathbf{x}) + \epsilon, \quad \epsilon \sim \mathcal{N}\left(0, \sigma^2\right), \tag{A.17}$$

where $f(\cdot)$ is drawn from a Gaussian process prior with constant mean and squared exponential covariance function. To address the $O(n^3)$ computational cost of exact inference, the model uses m inducing points $\mathbf{Z} = \{\mathbf{z}_1, \ldots, \mathbf{z}_m\}$ with $m \ll n$. The latent function is approximated using:

$$q(\mathbf{f}) = p(\mathbf{f}|\mathbf{u})q(\mathbf{u}), \quad q(\mathbf{u}) = \mathcal{N}(\mathbf{u}|\mathbf{m}, \mathbf{S}), \tag{A.18}$$

where $\mathbf{u} = f(\mathbf{Z})$ and $\mathbf{m}, \mathbf{S}$ are variational parameters. The covariance function is:

$$k(\mathbf{x}, \mathbf{x}') = \sigma_f^2 \exp\left(-\frac{|\mathbf{x} - \mathbf{x}'|^2}{2\ell^2}\right). \tag{A.19}$$

The model is trained by maximizing the evidence lower bound (ELBO):

$$\mathcal{L}(\theta) = \mathbb{E}_{q(\mathbf{f})}\left[\sum_{i=1}^{N} \log p(y_i|f_i)\right] - \mathrm{KL}(q(\mathbf{u})\|p(\mathbf{u})), \tag{A.20}$$

using the Adam optimizer from PyTorch. The implementation uses GPyTorch's `VariationalStrategy` and `CholeskyVariationalDistribution`, with inducing points initialized from training data and optimized during training.

Cite this article: Whiteley J and Becque J (2026). A Bayesian optimization approach for reliability-based design of prestressed concrete structures. *Data-Centric Engineering*, 7, e3. doi:10.1017/dce.2026.10037

https://doi.org/10.1017/dce.2026.10037 Published online by Cambridge University Press